Crystalline Structure and Morphology in Nylon-12: A Small- and Wide-Angle X-ray Scattering Study

Liangbin Li,[†] Michel H. J. Koch,[‡] and Wim H. de Jeu*,[†]

FOM-Institute for Atomic and Molecular Physics, Kruislaan 407, 1098 SJ Amsterdam, The Netherlands, and European Molecular Biology Laboratory, EMBL c/o DESY, Notkestrasse 85, D-22603 Hamburg, Germany

Received October 11, 2002; Revised Manuscript Received January 10, 2003

ABSTRACT: Simultaneous small- and wide-angle X-ray scattering has been employed to monitor the temperature dependence of the crystalline structure and morphology of nylon-12. Wide-angle measurements reveal that the α′-phase is a stable high-temperature crystalline phase. Upon cooling, a crystalline transition takes place from the α′-form into the hexagonal γ-phase. The small-angle data indicate at this point a discontinuous change in the density. At low temperatures, two crystal reflections occur at wide angles. This is interpreted as a monoclinic or an orthorhombic structure, which evolves from the hexagonal structure of the γ-form by an anisotropic thermal expansion. The evolution of the crystalline thickness during cooling and heating suggests the occurrences of partial surface crystallization and melting. This effect is superimposed on the transition α′ ↔ γ and leads to crystal thickening and thinning during cooling and heating, respectively. The transition from γ to α′ with increasing temperature arises from a "one-dimensional-melting" type of rupture between the hydrogen-bonded sheets. Finally, fast quenching from the melt results in the γ′-phase, which transforms upon annealing into either the γ- or the α′-polymorph. This process proceeds most probably through a melting and recrystallization process.

Introduction

Semicrystalline polymers typically consist of crystalline and amorphous domains with dimensions in the nanometer range, which form lamellar stacks in a superstructure of spherulites.[1] The final properties of such a polymer depend on the volume fraction of the crystalline domains as well as on their size and structure. In addition, the linkage between the crystals and the amorphous interlamellar regions is an important factor. In fact, all these effects are correlated. For example, changes on a length scale of 0.1 nm due to a crystalline transition may induce a morphological reorganization on a length scale of nanometers. Various phenomena can be expected to occur during such a crystalline transition. A different packing of the molecular chains in the different crystalline polymorphs leads to discontinuous changes in the density as well as in the equilibrium melting point. Also, differences in the mobility of the chains may affect the lamellar thickness, resulting in different morphologies.[2] Small-angle X-ray scattering (SAXS) is well suited to investigate these kinds of phenomena. Crystalline transitions can be detected from any discontinuity in the invariant Q and in the resulting morphological parameters.[3−6] In practice, however, semicrystalline polymers are complex, with a hierarchy of molecular interactions and structures displaying partial melting and recrystallization or secondary crystallization under the influence of temperature.[3,7−13] These effects can completely blur a discontinuity due to a crystalline transition. Nevertheless, the effect of crystalline transitions on the morphology has been clarified by SAXS in some specific situations. Murthy et al.[14] investigated the Brill transition in nylon-6.6 and found a change in the correlation length of the lamellae. Upon imposing orientation on poly(butylene terephthalate) the $\alpha \rightarrow \beta$ transition was observed.[15] In this paper we employ simultaneous SAXS and WAXS to explore the crystalline transitions and the corresponding morphological changes in nylon-12.

Crystalline transitions in nylon-12 have been investigated by WAXS, and so far four polymorphs have been reported, indicated as α, α′, γ, and γ′. The main crystal form obtained from the melt at atmospheric pressure is the γ-form, in which the amide plane is twisted out of the polymethylene plane by about 60°.[16] The γ′-form can be obtained by fast quenching from the melt and transforms into the γ-form upon annealing.[17] For both polymorphs a hexagonal structure was reported with only one strong reflection corresponding to a spacing of about 0.42 nm.[17] However, some authors found for the γ-form small deviations from hexagonal symmetry leading to a monoclinic unit cell with $\alpha = \beta = 90°$ and $\gamma = 120°-124.4°$. A monoclinic structure has been assigned to the α-form, which is obtained under specific conditions, such as high pressure or drawing.[18] A new α′-phase was recently observed by crystallization at high temperatures.[19] The amorphous density of nylon-12 is about 0.990 g/cm^3, while α- and γ-crystals have densities of 1.034 and 1.085 g/cm^3, respectively. Many details of the structures of these polymorphs and their mutual transformations are still unclear, while the amorphous region is even less well characterized. The concentration of hydrogen bonds in the amorphous regions and the premelting process of the crystals have been studied by NMR[20] and two-dimensional near-infrared correlation spectroscopy.[21,22] At increasing temperature, a conformational relaxation of the polymethylene segments occurs followed by rupture of hydrogen bonds, as revealed by the gradual increase in the number of free amide groups.

In this paper we present simultaneous SAXS and WAXS of the temperature dependence of crystalline structure and morphology of nylon-12. The objective is to investigate the influence of the crystalline structures

[†] FOM-Institute for Atomic and Molecular Physics.
[‡] European Molecular Biology Laboratory.
* Corresponding author: e-mail: dejeu@amolf.nl.

10.1021/ma025732l CCC: $25.00
Published on Web 02/14/2003

and their mutual transitions on the morphology. WAXS measurements indicate that upon lowering the temperature the distance between the hydrogen-bonded molecules decreases approximately linearly. In contrast, the distance between the hydrogen-bonded sheets displays two different slopes with a transition point around 110−130 °C. At this point discontinuous changes in the invariant and the crystalline thickness are observed in the SAXS intensity, which demonstrates the ability of SAXS to extract information on this crystalline transition.

Experimental Section

SAXS and WAXS Characterization. Nylon-12 was obtained from Aldrich and used as received. The melting point of this material is about 178 °C. A melting point up to about 209 °C has been reported for extended-chain crystals crystallized under high pressure.[23] Simultaneous SAXS and WAXS data were collected using the double focusing camera of beamline ×33[24] of the EMBL at Hasylab (DESY, Hamburg, Germany) at a wavelength of 0.15 nm. A data acquisition system[25] was used with two linear delay line detectors connected in series.[26] The SAXS region was calibrated using the first nine orders of dry calcified collagen and the WAXS region from the (120) and (112) reflections of poly(ethylene oxide). The SAXS and WAXS intensities were normalized to the intensity of the primary X-ray beam as measured by an ionization chamber placed upstream of the sample.

Additional WAXS and SAXS measurements were made using an in-house setup with a rotating anode X-ray generator (Rigaku RU-300H, 18 kW) equipped with two parabolic multilayer mirrors (Bruker, Karsruhe), giving a highly parallel beam of monochromatic Cu Kα radiation ($\lambda = 0.154$ nm) with a divergence of about 0.012°. The X-ray flux of this arrangement is an order of magnitude larger than for conventional pinhole collimation in combination with a nickel filter. The beam size was defined by two sets of slit pinholes while a guard slit pinhole was placed in front of the sample to cut parasitic scattering from the beam-defining slits and the mirrors. The SAXS intensity was collected with a two-dimensional gas-filled wire detector (Bruker Hi-star). A semitransparent beamstop in front of the area detector allowed us to monitor the intensity of the direct beam. The WAXS intensity was recorded by a linear position-sensitive detector (PSD-50M, M. Braun, Germany), which could be rotated around the beam path to measure in either the meridianal or the equatorial direction. The SAXS and WAXS intensities were normalized to the intensity of the direct beam attenuated by the semitransparent beamstop.

Experimental Procedure. A Linkam CSS450 temperature-controlled shear system was employed as sample stage. Samples were kept in a brass sample holder with Kapton windows replacing the original glass windows of the system. For isothermal crystallization the sample was first heated to 210 °C for 10 min and subsequently cooled to the crystallization temperature. At Hasylab, the SAXS and WAXS patterns were simultaneously recorded during crystallization in frames of 10 s. In some experiments the samples were first quenched from 210 °C to liquid nitrogen temperature followed by annealing at 60 °C. After completion of the crystallization or annealing, stepwise heating or cooling was applied.

Data Analysis. The two-dimensional SAXS intensity was first integrated azimuthally to obtain the scattering pattern as a function of $q = 4\pi \sin\theta/\lambda$, the modulus of the momentum transfer vector **q**, λ being the X-ray wavelength and 2θ the scattering angle. To examine the lamellar structures, linear correlation functions $\gamma(r)$[27−29] were calculated according to

$$\gamma(r) = \frac{1}{Q}\int_0^\infty I(q)q^2 \cos(qr)\, \mathrm{d}q \tag{1}$$

$$Q = \int_0^\infty I(q)q^2\, \mathrm{d}q \tag{2}$$

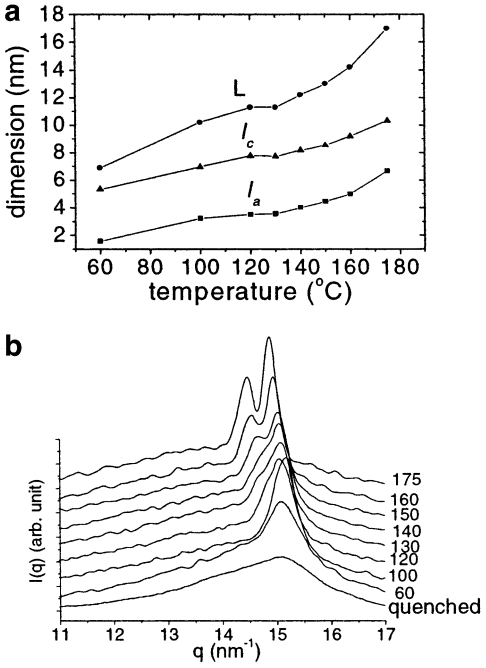

Figure 1. Results for nylon-12 samples isothermally crystallized at different temperatures. (a) Long period L, crystalline thickness l_c, and interlamellar amorphous thickness l_a, as obtained from SAXS measurements. (b) WAXS profiles; curves are shifted along the y-axis to clarify.

where Q is the so-called invariant. The correlation functions contain the basic morphological information for a model of lamellar stacks. The long spacing L can be estimated from the position of the first maximum. Further analysis of the correlation function yields the average crystalline lamellar thickness l_c and the amorphous layer thickness l_a. From these results the linear crystallinity $\phi_{cl} = l_c/L$ within the stacks can be calculated. However, analysis of the correlation function alone cannot tell which value of a subspacing belongs to l_c and which to l_a. We choose to assign the larger one to l_c because the other one is in some cases (see Figure 1a and Figure 9b) smaller than the crystalline unit cell dimension ($c \approx 3.2$ nm),[31] which is rather unreasonable. Moreover, for the alternative assignment the linear crystallinity ϕ_{cl} can be smaller than the apparent crystallinity, which is again unlikely. The invariant Q contains information on density contrast, which can be written as

$$Q \propto \phi_s(1 - \phi_{cl})\phi_{cl}(\rho_c - \rho_a)^2 \tag{3}$$

where ϕ_s is the volume fraction of lamellar stacks, and ρ_c and ρ_a are the densities of the crystalline and the amorphous parts, respectively. The volume crystallinity is given by $\phi_c = \phi_s\phi_{cl}$.

For each crystalline reflection in the WAXS profile, the integrated intensity, peak position, and peak width were obtained by fitting with two Gaussian functions. To describe the amorphous background, two additional broad Gaussians were needed. An estimate of the apparent crystallinity (by weight) A_c was obtained by dividing the sum of the intensities of the crystalline reflections I_c by the total intensity:

$$A_c = k\frac{\sum I_c}{\sum I_c + \sum I_a} = f(T)\phi_c = f(T)\phi_s\phi_{cl} \tag{4}$$

The apparent crystallinity is related to the volume crystallinity ϕ_c via $f(T)$. This empirical temperature-dependent factor accounts for minor corrections in the conversion of mass to volume crystallinity and the effects of thermal disorder, defects, and other factors that reduce the intensity of the crystalline peaks. Only a relative comparison will be made since neither A_c nor Q was determined on an absolute scale.

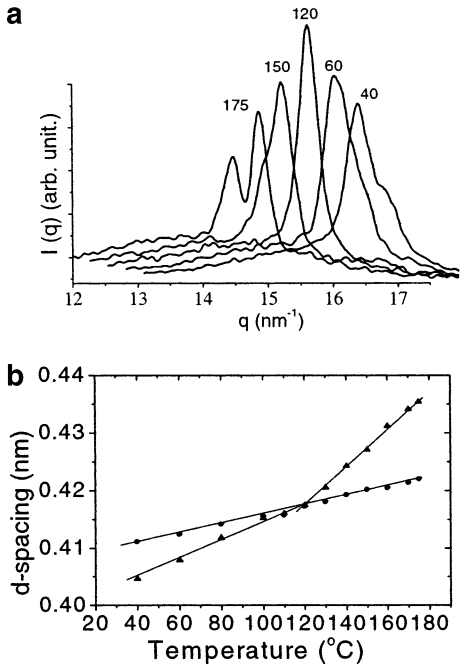

Figure 2. Results for sample I initially crystallized at 175 °C. (a) WAXS profiles at different temperatures; curves are shifted along *x*-axis to clarify. Measurements were taken during heating. (b) Resulting spacing between the hydrogen-bonded sheets (π) and the hydrogen-bonded molecular chains (☆).

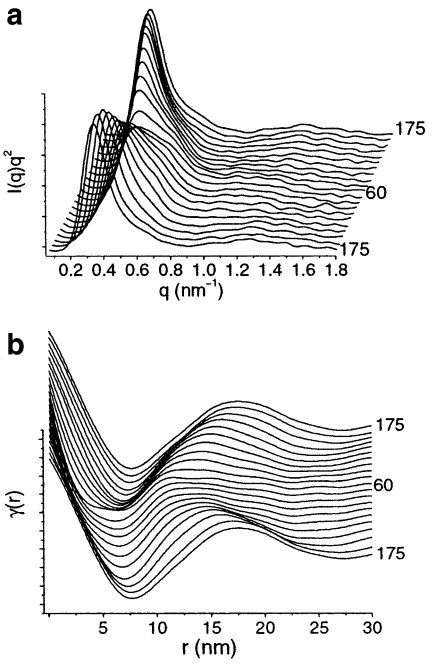

Figure 3. One-dimensional SAXS patterns (a) and calculated linear correlation functions (b) of sample I during subsequent stepwise cooling and heating.

Results

Isothermal Crystallization. Figure 1a displays the morphological parameters extracted from the SAXS patterns of samples isothermally crystallized at different temperature by cooling from the melt at 210 °C. The measurement at 60 °C was obtained by quenching to liquid nitrogen temperature followed by annealing at 60 °C. Because of the different thermal history, any comparison of this point with the others has to be treated with caution. The long period and crystalline and interlamellar amorphous thickness all decrease with decreasing crystallization temperature, in agreement with polymer crystallization theory.[30] Note that the long period and the crystalline thickness display an inflection point around 120 °C. Figure 1b gives the corresponding WAXS profiles. A WAXS pattern taken from the quenched sample is also presented Figure 1b, which shows a broad peak on the amorphous halo. At crystallization temperatures above 140 °C two reflections can be clearly distinguished, which are assigned to the α′-phase.[19] A single sharp reflection peak appears in the WAXS profiles of samples crystallized at lower temperatures, suggesting that under these conditions the hexagonal γ-form is obtained.[16] According to the literature, the sample quenched and annealed at 60 °C should be in the γ'-form.[17]

Heating and Cooling. Three samples with different thermal histories were used to study the temperature dependence of the crystalline structure and morphology. Starting points were the α′-form (sample I) and the γ-form (sample II), obtained by crystallization at high and low temperature, respectively, and the γ'-form (sample III), obtained by rapid quenching into liquid nitrogen.

The α′-Phase. Figure 2a displays the WAXS profiles of sample I as a function of temperature, starting from the α′-phase after crystallization at 175 °C. To highlight the shoulder on the high-q side of the reflection, the curves shown have been shifted by 20% along the q-axis. Apart from some thermal hysteresis, cooling and heating indicate a reversible process. Above 160 °C clearly two peaks are observed while at 140 °C a shoulder is still visible at the low-q side. In the temperature range between 100 and 130 °C only one sharp peak is found. Decreasing the temperature further to 80 °C, another small shoulder appears, now at the high-q side, which becomes quite pronounced at 40 °C. As the reflections progressively shift rather than simply disappear, systematically two Gaussians were used for fitting (see Figure 2b). The spacing corresponding to the distance between the hydrogen-bonded chains follows a single slope that increases linearly with temperature, while the distance between the hydrogen-bonded sheets has a different slope above and below 120 °C. Although we systematically fitted with two peaks, in the range 100−130 °C there might be only one reflection corresponding to hexagonal packing, restricted to this small temperature window. Figure 3 displays the Lorentz-corrected SAXS patterns and the corresponding correlation functions during stepwise cooling and subsequent heating. The morphological parameters, plotted in Figure 4a, are completely reversible within the experimental uncertainty and given the thermal hysteresis. An inflection point in l_c is observed around 120 °C, shown in more detail in Figure 4b. The invariant Q and the apparent crystallinity A_c are displayed in Figure 5.

The γ-Form. Sample II, crystallized at 100 °C, is typical for the γ-form. After complete crystallization the sample was cooled to 60 °C as a starting point for heating and cooling runs. The WAXS profiles during heating are shown in Figure 6. Above 140 °C two peaks can clearly be observed. At low temperatures a shoulder at the high-q side is found, as for the sample I that was originally in the α′-form. The apparent crystallinity A_c and invariant Q during heating and subsequent cooling are plotted in Figure 7. During cooling, a large jump occurs in A_c around 120 °C. The long period, crystalline

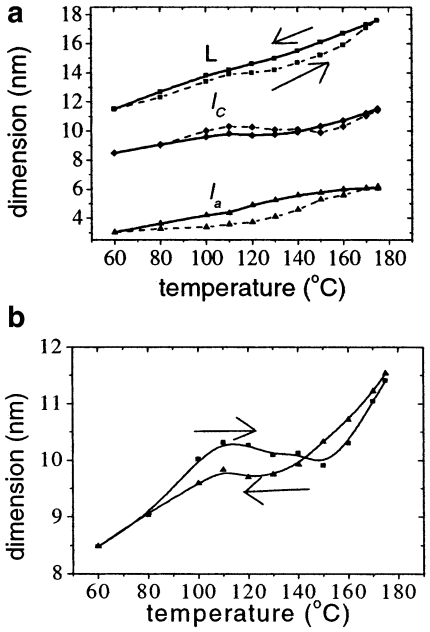

Figure 4. Long period L, crystalline thickness l_c, and interlamellar amorphous thickness l_a of sample I extracted from the correlation functions of Figure 3. (a) General behavior during cooling (solid line) and heating (dashed line). (b) Details of l_c around the crystalline transition during cooling (▲) and heating (■).

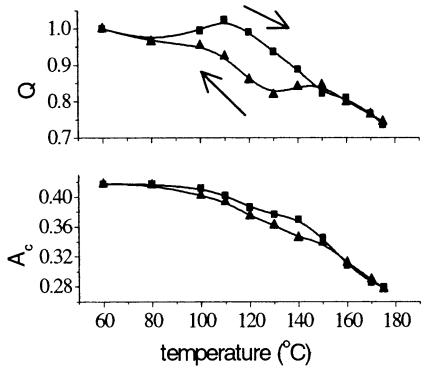

Figure 5. Apparent crystallinity A_c calculated from the WAXS and invariant Q calculated from the SAXS of sample I during stepwise cooling (▲) and subsequent heating (■).

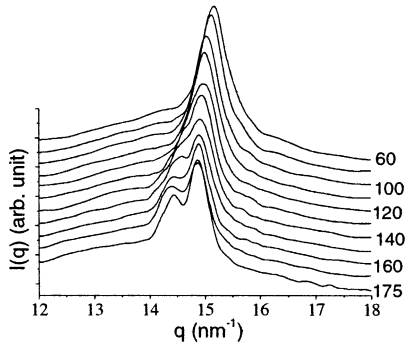

Figure 6. WAXS profiles of sample II, initially crystallized at 100 °C, during stepwise heating. Curves have been shifted along the y-axis for clarity.

thickness, and interlamellar amorphous thickness, as extracted from the correlation functions, are plotted in Figure 8. All morphological parameters increase with temperature. An inflection point can be seen around 120 °C, similar as for sample I (Figure 4a) though somewhat less pronounced.

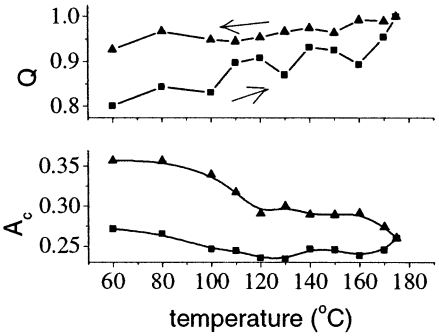

Figure 7. Apparent crystallinity A_c calculated from the WAXS and invariant Q calculated from the SAXS of sample II during stepwise heating (■) and subsequent cooling (▲).

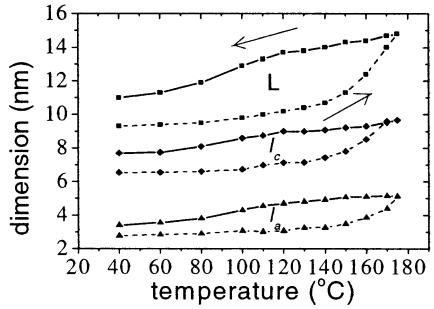

Figure 8. Long period L, crystalline thickness l_c, and interlamellar amorphous thickness l_a extracted from the linear correlation functions of sample II during stepwise heating (dashed line) and subsequent cooling (solid line).

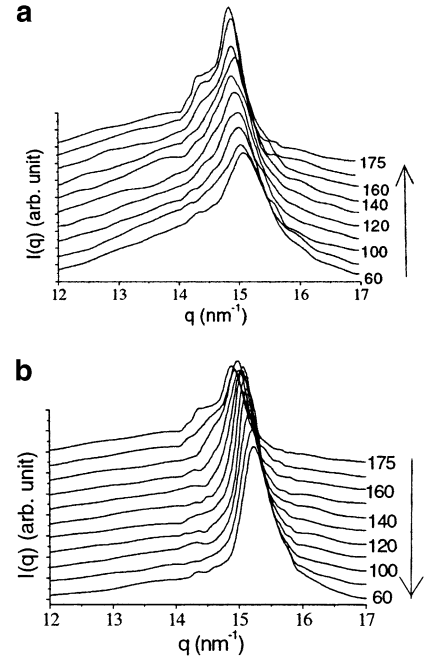

Figure 9. WAXS profiles of sample III, initially obtained by quenching, during stepwise heating (a) and subsequent cooling (b). Curves have been shifted along the y-axis for clarity.

The γ'-Form. Figure 9 displays the WAXS profiles during a stepwise heating and cooling of sample III, originally quenched in the γ'-form. Through the basic features during cooling and heating are similar, there is a clear asymmetry at the high-q side of the crystalline reflection after cooling. This suggests again two peaks exist at low temperatures. Above 140 °C a shoulder is observed at the low-q side. Figure 10 gives the morphological parameters obtained from the correlation func-

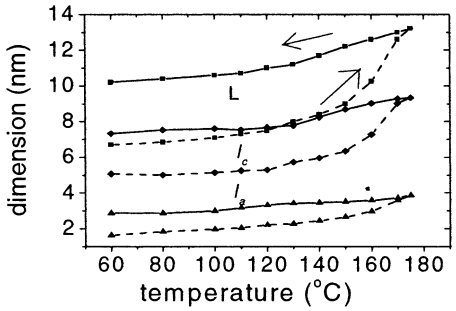

Figure 10. Long period L, crystalline thickness l_c, and interlamellar amorphous thickness l_a obtained from the linear correlation functions of sample III during stepwise heating (dashed line) and subsequent cooling (solid line).

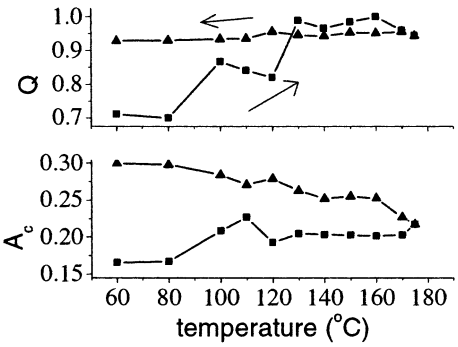

Figure 11. Apparent crystallinity A_c calculated from the WAXS and invariant Q calculated from the SAXS of sample III during stepwise heating (■) and subsequent cooling (▲).

tions of sample III during the first heating and cooling run. During heating a small increase in all morphological parameters in the lower-temperature range is followed by a larger increase between 140 and 175 °C. The long period increases by about 6 nm to approximately twice its original value. The heating and cooling effects are irreversible. After a full cycle, the thickness of the crystalline layers is appreciably larger than the original long period. Figure 11 illustrates the evolution of Q and A_c during heating and cooling.

Discussion

Crystalline Structures. The WAXS measurements of the three samples clearly indicate that the appearance of the so-called α′-phase does not depend on the original crystallization conditions. For all situations investigated (see Figures 2a, 6, and 9) it is a stable crystalline phase at high temperatures. The temperature dependence of the spacing in Figure 2b is very similar to that of double oriented nylon-12 samples.[31] However, the two-dimensional SAXS patterns indicate no preferred orientation in our case. By fitting with two Gaussians, we obtain different slopes for the spacing between the hydrogen-bonded sheets vs temperature at high and low temperatures. This result is somewhat artificial for the transition region, as between 100 and 130 °C also a high-quality fit is possible with one (hexagonal) peak. Most WAXS measurements reported so far were carried out at room temperature;[18] hence, differences may be due to differences in the thermal history. Our results confirm a structure with nonhexagonal packing after cooling to room temperature, which has been described as monoclinic from single crystal and fiber studies.[18,31−34] Our powder patterns also allow an orthorhombic lattice, which is the minimum requirement to generate two reflections. The two-dimensional

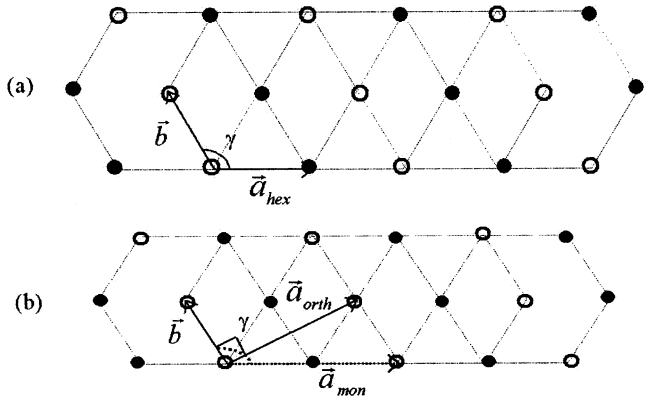

Figure 12. Two-dimensional lattice (*ab*-plane) of a nylon-12 crystal: (a) between 100 and 130 °C; (b) below 100 °C. Chains pointing up and down are indicated by solid and open circles, respectively. In the hexagonal (a) and the orthorhombic (b) lattice, the hydrogen bonds form sheets of directionally parallel chains, while they arrange in sheets of antiparallel chains in the monoclinic case.[18]

lattice (*ab*-plane) presented in Figure 12 indicates that the two WAXS peaks can be indexed as (200) and (110). At temperatures around 100−130 °C (see Figure 12) the lattice parameters $a \approx 0.833$ nm and $b \approx 0.481$ nm of the orthorhombic assignment fulfill the relation $a = b\sqrt{3}$, which corresponds to hexagonal packing. Upon decreasing the temperature, the distance between the hydrogen-bonded sheets decreases more rapidly than the one between the hydrogen-bonded chains (see Figure 12b) leading to $a < b\sqrt{3}$, and the structure becomes orthorhombic. For example, at 40 °C $a = 0.816$ nm, $b = 0.475$ nm, and $\alpha = \beta = \gamma = 90°$. However, the same WAXS data at 40 °C can also be fitted by a monoclinic structure with parameters $a = 0.955$ nm, $b = 0.469$ nm, and $\gamma = 120.6°$ (see Figure 12b), which is close to many of the reported cases.[32−34] The essential difference between these two possible structures is the orientation of the hydrogen bonds. The monoclinic structure assumes that the hydrogen bonds are parallel to the plane of polymethylene segments, while the orthorhombic lattice allows the hydrogen bonds to swing out of this plane with a nonzero angle, which is about 60° for hexagonal packing. In this picture the continuous shift from one to two reflections can be simply understood from the different temperature dependence of van der Waals forces and of hydrogen bonding (see Figure 12b), leading to a different thermal expansion in the two relevant directions. Further data are necessary to estimate the orientation of the hydrogen bonds; a monoclinic structure may still be possible.

The thermal expansion coefficients between the hydrogen-bonded sheets above and below about 120 °C are different, as indicated in the plot of *d*-spacing vs temperature (Figure 2b). We suppose that this transition point is correlated with the melting point of polyethylene. Generally, the amide groups and hydrogen bonds keep the bonded chains at a distance larger than expected in the absence of hydrogen bonds.[18] Hence, extrapolated to large n, the crystal density of n-nylons is expected to be consistently smaller than in polyethylene. Above 120 °C, the distance between the hydrogen-bonded sheets turns out to be larger than that between the hydrogen-bonded chains. As the transition temperature is comparable to the normal melting point of polyethylene, the sharp increase of the distance between hydrogen-bonded sheets can be attributed to a "one-

dimensional-melting" type of rupture between these sheets. Above 120 °C, the linear thermal expansion coefficient between the hydrogen-bonded sheets is about 8×10^{-4} °C^{-1}, which is about 1 order larger than the value at room temperature.[18] Two-dimensional near-infrared spectra of the premelting behavior of nylon-12 provide further support for this picture of "one-dimensional melting".[21,22] Dynamic spectra show that a band at 5770 cm^{-1} corresponding to CH_2 stretching vibrations switches from positive to negative around 110 °C.

On the basis of our WAXS measurements, a simple picture of the phase diagram of nylon-12 can be given. At high temperatures, nylon-12 is in the α′-phase, which is characterized by two crystalline reflections. The underlying structure still has to be solved, but on the basis of our powder measurements, it cannot have a higher symmetry than the orthorhombic. In the temperature range from about 100 to 130 °C, the hexagonally packed γ-form exists (one reflection). When the temperature is further lowered to 40 °C, two reflections appear again as a result of an anisotropic thermal expansion leading to at least an orthorhombic or probably a monoclinic structure.

Morphology and Changes in Q and A_c. In general, in semicrystalline polymers the long period and crystalline and interlamellar amorphous thickness all increase with temperature.[3,7−13] The various processes involved (melting/crystallization, expansion/contraction) work in opposite directions for heating/cooling, with the exception of thinning of crystals. In the case of nylon-12, a crystalline transition is superimposed on these phenomena. This transition is fully clear in sample I, which displays a reversible behavior during cooling and heating (see Figures 4 and 5). With decreasing temperature, secondary crystallization causes the crystallinity to increase continuously, while during heating partial melting occurs. Figure 5 reveals a discontinuous change of the density around the transition point. Both ρ_a and ρ_c increase with decreasing temperature, while near the crystalline transition the temperature dependence of ρ_c becomes weaker (Figure 2b), leading to a sharp decrease of $\Delta\rho$. According to eqs 3 and 4, this discontinuity shows up in a different behavior of Q and A_c, provided that the change in crystallinity is monotonic. When the temperature increases, the initial crystalline phase retains its density until the transition temperature is reached, while the density of the amorphous regions ρ_a already starts decreasing. This leads to an increase of Q before the transition point, whereas the decrease at the high-temperature side is due to a decrease of A_c (cf. Figure 5).

Sample II (γ-form) initially has a lower crystallinity and lamellar thickness than sample I (cf. Figures 4 and 8). During heating clearly partial melting and recrystallization occur. In Figure 7 the decrease in crystallinity during the first stage of heating is due to the melting of secondary crystals, as the sample was originally crystallized at 100 °C and cooled to 60 °C. In this situation it is almost impossible to extract information about the crystalline transition. The large jump in crystallinity around 120 °C during cooling is not reflected in the evolution of Q (Figure 7) although some changes occur in the slope of the l_c curve (Figure 8).

The γ′-form obtained by fast quenching is believed to consist of small crystals with many defects. This is confirmed for sample III by the broad and weak reflection in the WAXS profile and by the morphological parameters from the SAXS analysis (Figure 1). Sample III transforms into the γ-form upon annealing at temperatures above 110 °C.[17] The 10 min spent at each temperature during cycling should suffice to complete this transformation, as confirmed by the appearance of two crystalline reflections in the WAXS profiles (Figure 9). When the temperature is increased, the crystals become more perfect. At the initial stage of the process, molecular chains start relaxing and become sufficiently mobile to crystallize as indicated by the increase of A_c and Q (Figure 11). Around 110 °C both A_c and Q decrease, which corresponds to the transformation from the γ′-form to either the γ- or α′-phase. Because A_c and Q evolve in the same way—as predicted by eqs 3 and 4—the effect is most likely due to a change of ϕ_s. The evolution of A_c and Q during heating supports the view that the transition from the γ′-form occurs through partial melting and recrystallization. An even more pronounced increase in Q is due to the increase of $\Delta\rho = \rho_c - \rho_a$ with increasing temperature. During cooling, the crystallinity continuously increases, except at the inflection point at 120 °C. Interestingly, there is a similar inflection point in Q, which is otherwise relatively constant (Figure 11), perhaps as a result of a compensation between crystallinity and $\Delta\rho$.

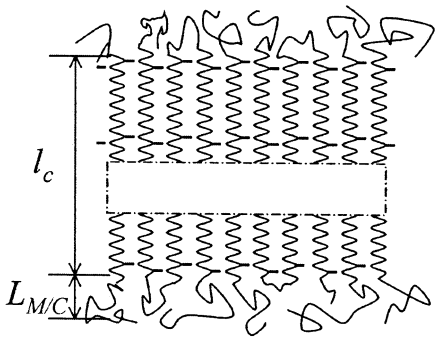

Figure 13. Surface melting and crystallization model of a nylon-12 crystal; $L_{M/C}$ indicates the region of melting and crystallization.

Surface Melting and Crystallization. An explanation of the behavior of the crystalline thickness l_c around the transition point (Figure 4b) is not straightforward. With decreasing temperature, secondary crystallization continuously fills the stacks with thinner lamellar crystals[19] as expressed in the increase of both A_c and Q (Figure 5). The average value of l_c, extracted from SAXS, is thus expected to decrease when the temperature lowered, which is indeed generally observed in semicrystalline polymers.[7−13] Deviations from this process in the vicinity of the transition point (illustrated in Figure 4b) indicate that crystal thickening may occur. This can be explained by Fischer's surface premelting model.[7] Molecular chains of nylon-12 contain relatively long methylene segments separated by short sections with amide groups as sketched in Figure 13. As far as the two strong hydrogen bonds allow, the methylene segment would remain preferentially in the molten state at least for temperatures above the equilibrium melting point of polyethylene (about 141 °C).[35] This results in lamellar crystals of nylon-12 with hydrogen bonds at the top and bottom surface. The methylene segment remain as cilia (or methylene brushes) in the interlamellar amorphous layer. When the temperature drops below 141 °C, these methylene brushes can easily be incorporated into the nylon-12 crystalline lattice by epitaxial growth. In addition to the cilia, tight folds also

exist on the surface, which require local reorganization at crystal thickening. Fischer's surface crystallization model requires the chains to become mobile in order to reorganize.[36] The crystalline transition may facilitate such a shift of the molecular chains and a local reorganization.[31] A high mobility may also be due to the hexagonal structure between 100 and 130 °C. Compared to less symmetric structures,[37,38] in polymer crystals a hexagonal packing corresponds quite generally to a relatively high molecular mobility. A typical example is the high-pressure hexagonal phase of polyethylene.[2] The temperature range in which the crystalline thickness changes is in agreement with this explanation. Taking the length of a methylene segment of a single nylon-12 unit, we estimate an increase in thickness of about 1 nm. This corresponds approximately to the deviation of l_c from a linear extrapolation in Figure 4b. The same mechanism applies to the hysteresis observed during heating.

Conclusions

On the basis of combined SAXS and WAXS results, we come to the following conclusions regarding nylon-12. (1) The α′-phase is a stable phase that occurs at high temperatures, independent of the thermal history. At temperatures around 100−130 °C a hexagonal phase exists (single WAXS peak). The evolution into two WAXS reflections at low temperatures can be explained by an orthorhombic or a monoclinic phase. (2) A crystalline transition $\gamma \leftrightarrow \alpha'$ occurs around 120 °C, for which a discontinuous change in density can be extracted from the evolution of the invariant Q of a well-defined sample. (3) The evolution of l_c during cooling and heating suggests that partial surface melting and crystallization occurs. This is superimposed on the crystalline transition, leading to thickening and thinning during cooling and heating, respectively. (4) The transition from the γ-phase to the α′-phase is interpreted as a "one-dimensional melting" type of rupture between the hydrogen-bonded sheets, while the transition from the γ′-phase to either the γ- or α′-form occurs most probably through melting and recrystallization. (5) Well-defined starting samples at high temperatures for which recrystallization can be avoided are essential to extract information about the crystalline transitions from SAXS.

Acknowledgment. The authors thank Y. Séréro, D. Lambreva, I. Sikharulidze, M. Al-Hussein, and W. Hu (Amsterdam) for valuable discussions. This work is part of the Softlink research program of the "Stichting voor Fundamenteel Onderzoek der Materie" (FOM), which is financially supported by the "Nederlandse Organisatie voor Wetenschappelijk Onderzoek" (NWO).

References and Notes

(1) Wunderlich, B. *Macromolecular Physics*; Academic Press: New York, 1970; Vol. 1.
(2) Rastogi, S.; Hikosaka, M.; Kawabata, H.; Keller, A. *Macromolecules* **1991**, *24*, 6384.
(3) Fischer, E. W. *Pure Appl. Chem.* **1971**, *26*, 385.
(4) Glatter, O.; Kratky, O. *Small-Angle X-ray Scattering*; Academic Press: New York, 1982.
(5) Russell, T. P. Small-Angle Scattering. In *Handbook on Synchrotron Radiation*; Brown, G. S., Moncton, D. E., Eds.; Elsevier Science: Amsterdam, 1991; Vol. 3.
(6) Chu, B.; Hsiao, B. S. *Chem. Rev.* **2001**, *101*, 1727.
(7) Fischer, E. W. *Pure Appl. Chem.* **1972**, *31*, 113.
(8) Kruger, K. N.; Zachmann, H. G. *Macromolecules* **1993**, *26*, 5202.
(9) Jonas, A. M.; Russell, T. P.; Yoon, D. Y. *Macromolecules* **1995**, *28*, 8491.
(10) Verma, R.; Marand, H.; Hsiao, B. S. *Macromolecules* **1996**, *29*, 7767.
(11) Fougnies, C.; Damman, P.; Villers, D.; Dosière, M.; Koch, M. H. J. *Macromolecules* **1997**, *30*, 1385.
(12) Dreezen, G.; Mischenko, N.; Koch, M. H. J.; Reynaers, H.; Groeninckx, G. *Macromolecules* **1999**, *32*, 4015.
(13) Wang, Z. G.; Hsiao, B. S.; Sauer, B.; Kampert, W. *Polymer* **1999**, *40*, 4615.
(14) Murthy, N. S.; Wang, Z. G.; Hsiao, B. S. *Macromolecules* **1999**, *32*, 5594.
(15) Apostolov, A. A.; Fakirov, S.; Stamm, M.; Patil, R. D.; Mark, J. E. *Macromolecules* **2000**, *33*, 6856.
(16) Arimoto, H.; Ishibashi, M.; Hirai, M.; Chatani, Y. *J. Polym. Sci.* **1965**, *A3*, 317.
(17) Hiramatsu, N.; Haraguchi, K.; Hirakawa, S. *Jpn. J. Appl. Phys.* **1983**, *22*, 335.
(18) Aharoni, S. M. *n-Nylons: Their Synthesis, Structure and Properties*; John Wiley & Sons: Chichester, 1997; Chapters 1.3 and 2.12.
(19) Ramesh, C. *Macromolecules* **1999**, *32*, 5704.
(20) Mathias, L. J.; Johnson, C. G. *Macromolecules* **1991**, *24*, 6114.
(21) Ozaki, Y.; Liu, Y. L.; Noda, I. *Macromolecules* **1997**, *30*, 2391.
(22) Czarnecki, M. A.; Wu, P. Y.; Siesler, H. W. *Chem. Phys. Lett.* **1998**, *283*, 326.
(23) Stamhuis, J. E.; Pennings, A. J. *Polymer* **1977**, *18*, 667.
(24) Koch, M. H. J.; Bordas, J. *Nucl. Instrum. Methods* **1983**, *208*, 461.
(25) Boulin, C. J.; Kempf, R.; Gabriel, A.; Koch, M. H. J. *Nucl. Instrum. Methods* **1988**, *A269*, 312.
(26) Rapp, G.; Gabriel, A.; Dosiere, M.; Koch, M. H. J. *Nucl. Instrum. Methods* **1995**, *A357*, 178.
(27) Vonk, C.; Kortleve, G. *Kolloid Z. Z. Polym.* **1967**, *220*, 19.
(28) Strobl, G. R.; Schneider, M. *J. Polym. Sci., Polym. Phys. Ed.* **1980**, *18*, 1343.
(29) Goderis, B.; Reynaers, H.; Koch, M. H. J.; Mathot, V. B. F. *J. Polym. Sci., Part B: Polym. Phys.* **1999**, *37*, 1715.
(30) Wunderlich, B. *Macromolecular Physics*; Academic Press: New York, 1973; Vol. 2.
(31) Dosière, M. *Polymer* **1993**, *34*, 3160.
(32) Northolt, M. G.; Tabor, B.; van Aartsen, J. J. *J. Polym. Sci., Part A-2* **1972**, *10*, 191.
(33) Cojazzi, G.; et al. *Makromol. Chem.* **1973**, *168*, 289.
(34) Inoue, K.; Hoshino, S. *J. Polym. Sci., Part A-2* **1973**, *11*, 1077.
(35) Wunderlich, B. *Macromolecular Physics*; Academic Press: New York, 1980; Vol. 3.
(36) Hu, H.; Albrecht, T.; Strobl, G. *Macromolecules* **1999**, *32*, 7548.
(37) Wunderlich, B.; Moller, M.; Grebowicz, J.; Baur, H. *Conformational Motion and Disorder in Low and High Molecular Mass Crystals*; Springer-Verlag: Berlin, 1988.
(38) Ungar, G. *Polymer* **1993**, *34*, 2050.

MA025732L